minerals

MDPI

Article

Flotation Depression of Arsenopyrite Using Sodium Nitrobenzoate under Alkaline Conditions

Xiaohao Sun [1], Bozeng Wu [1,*], Mingzhen Hu [2,3], Hongxin Qiu [1], Jiushuai Deng [1], Jiaozong Cai [1] and Xiaoli Jin [1]

[1] School of Chemical and Environmental Engineering, China University of Mining and Technology-Beijing, Beijing 100083, China; Bqt1900301006@student.cumtb.edu.cn (X.S.); Bqt2100301011@student.cumtb.edu.cn (H.Q.); 202001@cumtb.edu.cn (J.D.); Bqt2000301011@student.cumtb.edu.cn (J.C.); zqt1900301006@student.cumtb.edu.cn (X.J.)
[2] Liuzhou China-Tin Nonferrous Design and Research Institute Co., Ltd., China Tin Group Co., Liuzhou 545000, China; hmz369hn@126.com
[3] National Engineering Laboratory for Efficient Utilization of Indium and Tin Resources, China Tin Group Co., Liuzhou 545000, China
* Correspondence: wubz998@163.com

Abstract: Arsenopyrite is a common arsenic-containing mineral that is often closely associated with sulfide minerals, such as pyrite, chalcopyrite, pyrrhotite, galena, and sphalerite, and with precious metals, such as gold and silver. The selective inhibition of arsenopyrite is an important method used to reduce the arsenic content of processed products, the cost of arsenic removal in metallurgical processes, and its impact on the environment. In this study, we discovered a chemical sodium, m-nitrobenzoate (m-NBO), that can effectively inhibit the flotation behaviors of arsenopyrite via sodium butyl xanthate (NaBX), and these effects were studied by flotation experiments. The results showed that, using NaBX as a collector, arsenopyrite had good floatability under acidic conditions, but the floatability decreased under alkaline conditions. Furthermore, the organic inhibitor m-NBO had a significant inhibitory effect on arsenopyrite under alkaline conditions. In addition, the adsorption between m-NBO and NaBX was competitive, and a hydrophilic layer formed on the surface of arsenopyrite. The passivation film prevents dixanthogen from being adsorbed on the surface of the mineral. Due to the effect of m-NBO on arsenopyrite, the redox potential and oxide content of the arsenopyrite surface increased, the hydrophobicity of the arsenopyrite surface was reduced, and the flotation of arsenopyrite was inhibited. These results provide options for separating multimetal sulfide minerals and arsenic-containing minerals.

Keywords: flotation; arsenopyrite; m-NBO; surface properties; depression; redox potential

Citation: Sun, X.; Wu, B.; Hu, M.; Qiu, H.; Deng, J.; Cai, J.; Jin, X. Flotation Depression of Arsenopyrite Using Sodium Nitrobenzoate under Alkaline Conditions. *Minerals* **2021**, *11*, 1216. https://doi.org/10.3390/min11111216

Academic Editor: Przemyslaw B. Kowalczuk

Received: 29 September 2021
Accepted: 27 October 2021
Published: 30 October 2021

1. Introduction

Arsenic is a pollutant that affects waterbodies and soil [1]. It can be stabilized as a series of pentavalent (arsenate) anions: H_3AsO^{4-}, H_2AsO^{4-}, $HAsO_4^{2-}$, and AsO^{4-}. However, under most reducing (acidic and weakly alkaline) conditions and lower redox potentials, trivalent arsenate (H_3AsO_3) dominates. Due to its instability, arsenic has become a significant source of arsenic pollution in the environment [2].

From the perspective of thermodynamics, arsenopyrite is easily oxidized and decomposed in both acid and alkaline media, but from the perspective of kinetics, arsenopyrite is an inert mineral that is difficult to oxidize [3]. As the oxidation process of arsenopyrite is a process that converts S, As, and Fe from low valence to high valence, passivation films form on the surface, limiting arsenopyrite oxidation to a certain extent [4]. Once arsenopyrite is oxidized, it releases Fe, As, S, and other elements. Among them, special attention should be paid to As and its valence state because arsenic is a toxic element, and its toxicity is related to its valence, especially As^{3+} and As^{5+}. In a supergene

environment system, because the environment is rich in oxygen, arsenopyrite decomposition is inevitable and pollutes the surrounding environment [5]. Therefore, separating arsenic from other minerals in the form of arsenopyrite as a part of tailing filling in mining processes can reduce the environmental pollution caused by the release of arsenic due to the oxidative decomposition of arsenopyrite.

The most common mineral in arsenic-bearing minerals is arsenopyrite, which is often closely associated with sulfide minerals, such as pyrite, chalcopyrite, pyrrhotite, galena, and sphalerite [6]. In the process of nonferrous metal mineral recovery, the [Fe–S] bond exposed during the dissociation of arsenopyrite can easily interact with thio-compound collectors and can enter the flotation concentrate of sulfide minerals, resulting in arsenic being present in the main metal concentrate and in the arsenic content exceeding the standard and affecting the quality of the concentrate. In the subsequent smelting process, the smelting cost increases due to the removal of arsenic [7,8]. We take tin smelting in Guangxi, China, as an example, as this industry is the most advantageous and is characteristic of the area. A large amount of arsenic-containing gypsum slag is produced during pyrometallurgical smelting. In the process of arsenic removal, every 1 ton of arsenic removed carries away 3 to 4 tons of tin, resulting in a huge waste of tin resources. In Australia, because of strict arsenic emission standards, smelters only process copper concentrates with <0.5% arsenic, because each 0.1 wt% higher of arsenic is fined at about USD 3 [5,9]. Therefore, the effective separation of arsenic-containing minerals, such as arsenopyrite and other sulfide minerals, in the process of beneficiation of nonferrous metal sulfide minerals is crucial.

As arsenopyrite is also a type of sulfide mineral, the similarities between its crystal structure and surface bond energy, and those of the co-associated sulfide minerals cause similar flotation thermodynamic properties. Therefore, their separation is difficult and has remained problematic in beneficiation work [10]. Over the years, researchers have conducted a lot of research to reduce the arsenic content in sulfide minerals. Although the technologies used to inhibit arsenopyrite with inorganic inhibitors are relatively mature [11,12], the depletion of nonferrous resources, the quality of the concentrate, and the need to protect the environment now involve increasingly stringent measures. In addition, the selective inhibitory effect of inorganic inhibitors on arsenopyrite has various problems such as a large dosage, poor selectivity, and large impact on subsequent processes. Therefore, alternative agents with good selectivity and a good inhibitory effect are still needed. Organic inhibitors have multiple functionalities to meet various needs, such as a reduction ability, a coordination ability, hydrophilicity, high flexibility, low cost, environmental friendliness, and good selectivity. Therefore, in recent years, organic chemicals have been favored by engineers and researchers in mineral processing [13]. Specifically, this concerns the development of high-efficiency small molecule organic inhibitors with multifunctional groups, which are also a feasible way to meet the needs of resource development, to meet new environmental protection requirements, and to reduce smelting costs [14].

In recent years, surface spectroscopy and electrochemical methods have been widely used to study the process of minerals and flotation reagents [15]. Studies have shown that there are two mechanisms of inhibiting arsenopyrite [16,17]. In the first mechanism, under alkaline conditions, the oxidation potential is reached in the presence of an oxidant. The appearance of an oxidation potential causes arsenopyrite to form a film of iron hydroxide on the surface, thereby inhibiting arsenopyrite. In the second mechanism, a large number of hydroxyl and carboxyl groups are present in the molecular structure of the inhibitor. In an alkaline medium, some of the groups interact with the minerals and are chemically adsorbed on the surface of arsenopyrite in the form of anions, forming a hydrophilic film that prevents and covers the role of collectors, which makes arsenopyrite hydrophilic. On this basis, many previous works studied amino trimethyl phosphonic acid, ethylenediamine tetra-n-propionic acid, ethylenediamine tetramethylene phosphonic

acid, pyrogallic acid, hydroquinone, tannic acid, α-amino phosphoric acid [18], benzodiazepines [19], and new organic small molecule inhibitors.

Under the action of polar functional groups, when interacting with minerals, some of the polar groups in the molecule selectively interact with the surface of minerals. This process extends outwards to the medium (water), causing the surface of minerals to be hydrophilic or preventing the adsorption of collectors, thereby inhibiting the flotation of the minerals [20]. When macromolecular organic inhibitors interact with minerals, a hydrophilic adsorption layer is formed and the collectors adsorbed on the mineral surface are masked. These processes result in shielding of the collector hydrophobic effect and cause the mineral to be hydrophilic and inhibited. Therefore, tannin [21], HA sodium (ammonium) [22], polyacrylamide [13], lignosulfonate [23], and organic macromolecular inhibitors have good applications in the removal of arsenopyrite.

Nitrobenzoate, which is an organic oxidant, has certain corrosive properties to metals at low concentrations. Its corrosion form is localized corrosion [24]. Although As is semimetallic and S is nonmetallic, arsenopyrite is a semiconductor, similar to an "alloy" [25]. However, in essence, an arsenopyrite oxidation process occurs with or without inhibitors in a flotation system. Therefore, linking the oxidation process of arsenopyrite with the "corrosion" process of the alloy-like arsenopyrite and the process of achieving "passivation" of arsenopyrite by forming a passivation film on its surface is easy. The use of electrochemical technology to study the electrochemical behavior of FeAsS in the required electrolyte, especially the oxidation process, is without a double of great significance [26].

Based on the two aforementioned, important points (organic agent and arsenopyrite oxidization), this study found a small organic molecule inhibitor agent that has oxidizing properties and that can have a significant inhibitory effect on arsenopyrite sodium m-nitrobenzoate (m-NBO) [27]. Herein, we used Fourier-transform infrared spectroscopy (FTIR), X-ray photoelectron spectroscopy (XPS), cyclic voltammetry curves (CV), and Tafel curves (Tafel) to study the m-NBO inhibitory mechanism of arsenopyrite.

2. Materials and Methods

2.1. Materials

The high-purity arsenopyrite sample was obtained from the Chifeng polymetallic sulfide deposit in Inner Mongolia [28]. Arsenopyrite (Apy) was manually selected, crushed, agate ground, and sieved. Next, 38–75 μm arsenopyrite samples were used for single mineral flotation, and 20–38 μm samples were used for the Fourier-transform infrared spectroscopy (FTIR) and X-ray photoelectron spectroscopy (XPS) analyses and the electrical preparation of the chemical powder electrodes. The main mass fraction of arsenopyrite is shown in Table 1. Among them, Fe, As, and S are the main elements, and their contents are 34.93 wt% Fe, 47.12 wt% As, and 14.88 wt% S. As seen from Table 1, the arsenopyrite sample used in this study has high purity and few impurity elements, and thus, it can be used in pure mineral test research.

Table 1. Chemical element analysis of arsenopyrite.

Element	Fe	As	S	Si	Zn	Al	Ca	Mn	K	P
Content (wt.%)	34.93	47.12	14.88	1.37	0.64	0.51	0.48	0.03	0.03	0.01

The reagents used in this study include inhibitors, collectors, and frothers. The inhibitor was the analytical reagent m-NBO produced by Shanghai Macklin Biochemical Co., Ltd. (Shanghai, China) and the collector NaBX was provided by Chehe Mineral Flotation Plant in Chehe, China (NaBX, purity > 85%). The foaming agent, terpineol oil, was provided by Tangshan Jest Technology Co., Ltd. (Tangshan, China). The other reagents in the test were analytically pure, including sodium hydroxide (NaOH),

hydrochloric acid (HCl), and other pH adjusters. Deionized water (resistivity: 18.2 MΩ) was used for all flotation and analytical studies.

2.2. Methods

2.2.1. Micro-flotation Tests

A total of 2 g of Apy was added to a 40 mL flotation cell for micro-flotation tests. The flotation behavior of arsenopyrite was then studied in different slurry systems under different pH conditions. Before the test, the mineral surface was treated with an ultrasonic cleaning apparatus for 3 min. The arsenopyrite samples treated in different ways were stirred for 2 min under specified solution conditions to enhance the interaction between the agent and the mineral. The pH value was measured with a pH meter (FE 20, METTLER TOLEDO, Zurich, Switzerland), and the pH of the suspension was adjusted as necessary using NaOH and HCl. Subsequently, various reagents were added to the pulp: m-NBO (if needed), NaBX (if needed), and terpineol. After 2 min flotation, the float and the sink products were collected and dried. Finally, the recovery rate was calculated based on the dry weight of the product [22]. The tests under the same conditions were conducted three times.

2.2.2. FTIR Measurements

The infrared spectrum analysis used a Nicolet IS 10 Fourier transform infrared spectrometer from Thermo Fisher Scientific (Waltham, MA, USA), with a scanning range of 4000–400 cm^{-1}. Each spectrum was scanned 16 times, and the measurement resolution was 4 cm^{-1}. For each analysis, 2 g of the sample was added to 40 mL of deionized water to adjust the pH. According to the needs, different reagents were added to the slurry, including m-NBO and NaBX. After the treatment, the sample was rinsed with deionized water three times and dried in a vacuum oven at 25 °C. For infrared spectroscopy analysis, 10 mg of the sample and 100 mg of spectral pure KBr were taken, uniformly mixed, and compressed into pellet with a tablet press [29].

2.2.3. XPS Measurements

XPS analysis was performed using an American Thermo Scientific K-Alpha plus (Waltham, MA, USA) and single chromium Al Kα x-ray source. The source energy was 1486.6 eV, the voltage was 15 kV, the beam current was 15 mA, and constant analyzer energy was analyzed in the (Constant Analyzer Energy) mode. All elements in the measurement sample were detected by survey scanning, and the high-resolution XPS spectra of C1s, Fe2p, S2p, As3d were recorded. All XPS spectra were fitted, analyzed, and calculated on Advantage software. All data were based on the C1s peak of surface contamination, the binding energy of which is 284.8 eV [22].

2.2.4. Electrochemical Measurements

In this work, CV curve and Tafel curve tests were performed to understand the interaction between m-NBO, NaBX, and arsenopyrite. The CHI 760E (CH Instruments, Inc., Austin, TX, USA) scanning electrochemical instrument is a traditional three-electrode electrochemical cell. Herein, a double-wall glass reactor was used as an electrochemical cell with an effective volume of 200 mL. The electrode was a mineral powder microelectrode, Ag/AgCl was used as a reference electrode, a glassy carbon electrode was used as a working electrode, and a graphite electrode was used as an auxiliary electrode. The electrolyte is 0.1 M KCl, and a 1 M NaOH solution adjusted the pH to pH = 9 and pH = 11.5 [30].

An open circuit potential (OCP) scan was performed before each CV experiment and started when the OCP stabilized (approximately 10 min later). In the CV study, the following cycle was performed: from the OCP to 600 mV (positive potential sweep), then to −800 mV (negative potential sweep), and then to the OCP at a sweep rate of 20 mV/s.

Each test was carried out for four cycles. The shape and peak intensity of the oxidation or reduction products became stable starting from the second scan, so the second test data were used. The Tafel test voltage range was OCP ± 0.3 V, and the scanning speed was 10 mV/s. The potentials above are all Ag/AgCl. According to the float test procedure, the reagents were added in the order of m-NBO (if needed) and NaBX (if needed). The arsenopyrite powder electrode was placed in the electrolyte for 15 min to reach equilibrium before the electrochemical measurement. The background electrolyte was 0.1 M KCl, and the pH value was adjusted to 11.5 using a NaOH solution [31].

3. Results and Discussion

3.1. Arsenopyrite Flotation Experiments

As shown in Figure 1, in order to verify the influence of m-NBO on the floatability of arsenopyrite, a series of flotation tests were carried out. The pH value and the type of agent play important roles in the flotation of arsenopyrite, and the determination of the optimal pH value depends on the lower recovery rate of arsenopyrite. When the pH value changed from 3 to 11, the selectivity of arsenopyrite decreased. Under lower pH conditions, arsenopyrite had a higher recovery rate under different flotation slurry systems. When pH = 3, the recovery rate of arsenopyrite was 40%. When 1.6×10^{-3} mol·L^{-1} of NaBX was added to the pulp, the recovery rate of arsenopyrite was 85%. When 50 mol·L^{-1} of m-NBO and 1.6×10^{-3} mol·L^{-1} of NaBX were added, the recovery rate of arsenopyrite was 78%. When pH > 9, the flotation recovery rate of arsenopyrite showed a downward trend, except for in the NaBX slurry systems, and when pH = 11.5, the recovery of arsenopyrite was the lowest. Due to the presence of polar groups such as m-NBO carboxyl and nitro groups, the Fe^{2+} or As^{3+} on the surface of arsenopyrite can be easily oxidized and fixed on the surface of minerals. The m-NBO molecules adsorbed by arsenopyrite form hydrogen bonds with water, thereby selectively suppressing arsenopyrite [13]. As shown in Figure 1, when m-NBO is present, the recovery rate of arsenopyrite drops sharply in pH = 11.5 conditions. These results show that m-NBO can change the surface properties of arsenopyrite under alkaline conditions and can reduce the floatability of arsenopyrite.

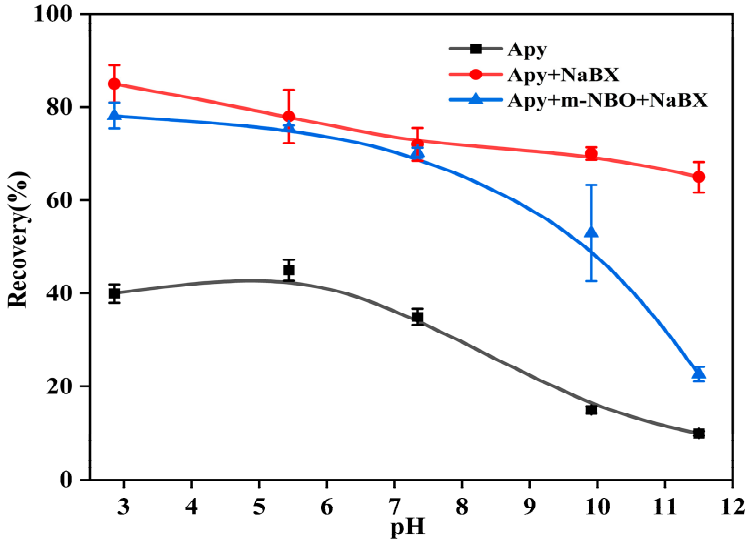

Figure 1. Effect of pH and depressants on the floatability of arsenopyrite, and error bar; C(m-NBO) = 50 mg·L^{-1} and C(NaBX) = 1.6×10^{-3} mol·L^{-1}.

As shown in Figure 2, as the amount of m-NBO increases, the recovery rate of arsenopyrite gradually decreases, but when C(m-NBO) > 50 mg/L, the recovery rate of arsenopyrite rises slightly, which may be due to the influence of competitive adsorption

between m-NBO and NaBX. It can also be seen from Figure 2 that, when the dosage of the agent is 50 mg/L, the recovery of arsenopyrite is the lowest.

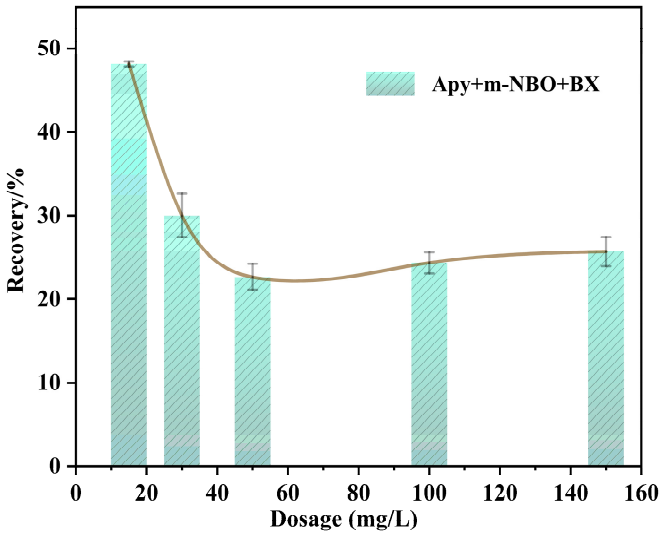

Figure 2. Effect of m-NBO dosage on the floatability of arsenopyrite, and error bar; C(NaBX) = 1.6 × 10^{-3} mol·L^{-1}, and pH = 11.5.

3.2. FTIR Analysis

Diffuse reflectance FTIR infrared spectroscopy was used to study the mechanism of action between m-NBO and arsenopyrite. The FTIR of organic inhibitor m-NBO is shown in Figure 3. Some obvious characteristic peaks can be observed, of which 3584 cm^{-1} is the broad peak-hydroxy stretching vibration and 3086 cm^{-1} is the –C–H– stretching vibration. At 1639 cm^{-1}, the vibration is –C=O– aromatic antisymmetric stretching. Furthermore, 1608 cm^{-1} corresponds to the C=C skeleton vibration of the aromatic ring, 1522 cm^{-1} and 1567 cm^{-1} correspond to the asymmetric vibrations of –NOO–, 1394 cm^{-1} and 1350 cm^{-1} correspond to the –NOO– symmetrical stretching vibrations or methyl deformation or to –COO– anti-symmetric stretching, 829 cm^{-1} corresponds to –C–H– out-of-plane bending vibrations, 790 cm^{-1} corresponds to the out-of-plane bending of the aromatic ring –C–H–, and 721 cm^{-1} corresponds to the binary substitution (meta) of benzene [32]. These results show that the molecular structure of m-NBO contains a variety of functional groups such as –COO– and –NOO–, and the reasonable combination of multiple functional groups matches the Benzene ring structure, so that m-NBO can be selectively adsorbed on the surface of minerals.

The FTIR of NaBX is shown in Figure 4, and the characteristic peak is 1108 cm^{-1}.

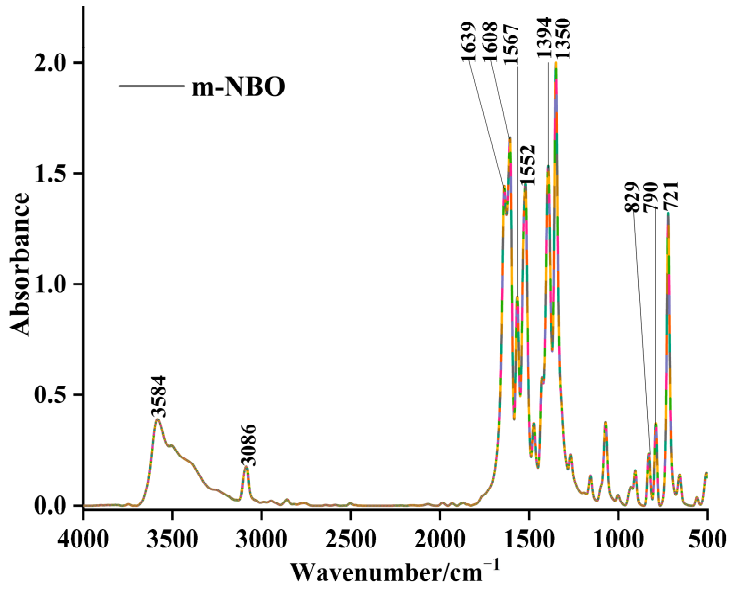

Figure 3. FTIR of organic-depressant m-NBO.

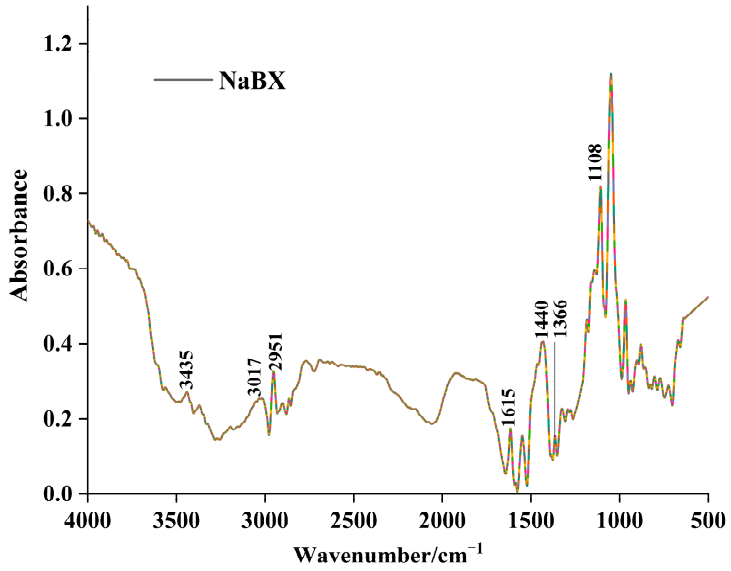

Figure 4. FTIR of NaBX.

Figure 5 shows the flotation effect of m-NBO on the flotation behavior of arsenopyrite. As can be observed from Figure 5, the results are quite different. The surface species produced by the interaction of arsenopyrite with m-NBO and NaBX were identified using infrared spectra. As shown in Figure 5 and Table 2, 3436 cm^{-1} and 1630 cm^{-1} bending vibrations of –O–H appear. These are mainly from the adsorption layer containing water on the surface of arsenopyrite. At 1049 cm^{-1}, 871 cm^{-1}, 580 cm^{-1}, and 431 cm^{-1}, the characteristic peaks of arsenopyrite are the SO_4^{2-} antisymmetric stretching vibration, As–O stretching vibration, Fe–O stretching vibration, and O–As–O bending vibration.

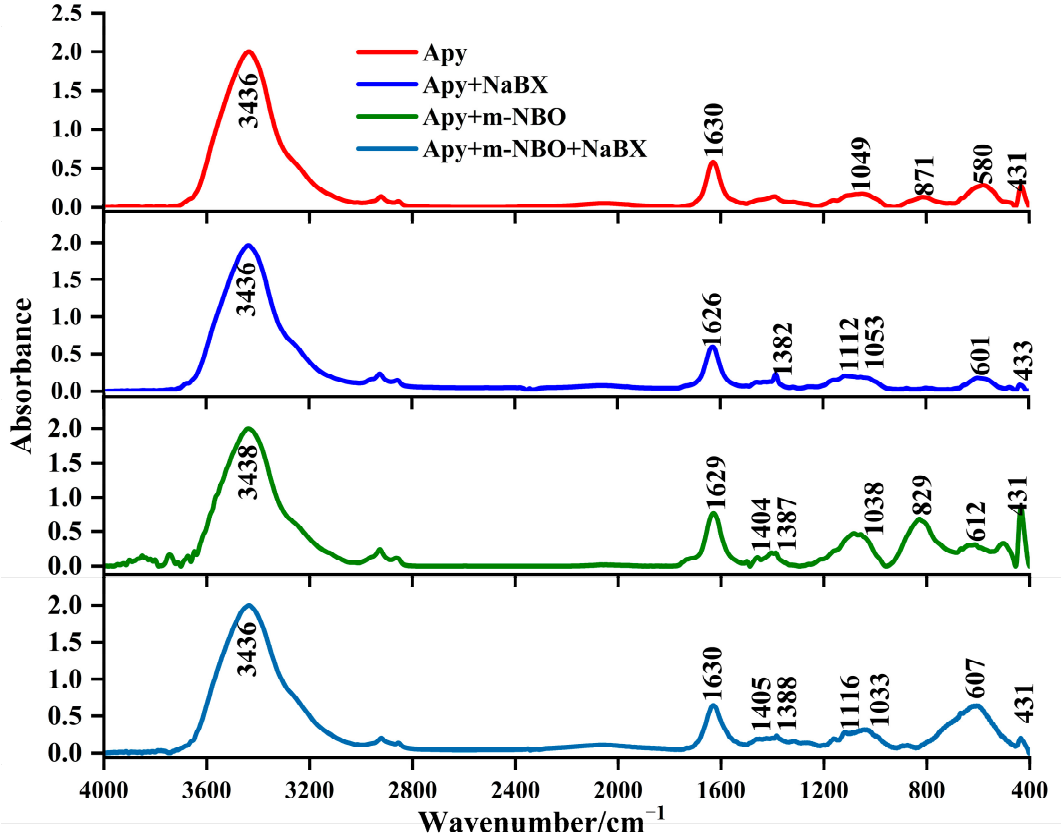

Figure 5. FTIR of arsenopyrite after interaction with m-NBO and NaBX; pH = 11.5, $C_{(m\text{-}NBO)}$ = 50 mg·L^{-1}, $C_{(NaBX)}$ =·1.6 × 10^{-3}·mol·L^{-1}.

The infrared spectra and band assignments before and after the action of arsenopyrite and the agent are shown in Figure 5 and Table 2.

When arsenopyrite reacts with NaBX, new absorption peaks appear at 1382 cm^{-1} and 1112 cm^{-1} in the infrared spectrum, indicating that NaBX has been adsorbed on the surface of arsenopyrite. Fornasiero et al. [33] believes that, in the alkaline pH range, xanthate can be oxidized into dixanthate and that it can also be oxidized into dixanthate by Fe^{3+} or $Fe(OH)_3$ particles, as shown in Equations (1) and (2):

$$2Fe^{3+} + 2EX^{-} \rightarrow 2Fe^{2+} + (EX)_2 \quad (1)$$

$$2Fe(OH)_3 + 6H^{+} + 2EX^{-} \rightarrow 2Fe^{2+} + 6H_2O + (EX)_2 \quad (2)$$

This further indicates that the hydrophobic product of NaBX on the surface of arsenopyrite is dixanthate and that its adsorption mode is a chemical action.

Table 2. Band assignments for arsenopyrite infrared spectrum features of m-NBO and NaBX (/ means none).

Apy	Apy + NaBX	Wavenumber/cm^{-1}		Functional Groups	Bonding Properties
		Apy + m-NBO	Apy + m-NBO + NaBX		
3436	3436	3438	3436	O–H bending vibrations	water (adsorbed water)
1630	1626	1629	1630	O–H bending vibrations	water (adsorbed water)
/	/	1404, 1387	1405, 1388	–NO_2 symmetrical stretching vibration	m-NBO
/	1382	/	/	–CH_3 bending vibrations	NaBX
/	1112	/	1116	C=S stretching vibration	NaBX
1049	1053	1083	1033	SO_4^{2-} stretch vibration	Apy
871	/	829	/	As–O stretching vibration	Apy
580	601	612	607	Fe–O stretching vibration	Apy
431	431	433	434	O–As–O bending vibrations	Apy

However, as shown in Figure 5, when arsenopyrite reacts with m-NBO, characteristic peaks of –NOO– appear at 1387 cm^{-1} and 1404 cm^{-1}, indicating that m-NBO is adsorbed on the surface of arsenopyrite. m-NBO complexes with the As and Fe ions on the surface of arsenopyrite to achieve chemical adsorption. The possible complexation reaction is shown in Figure 6.

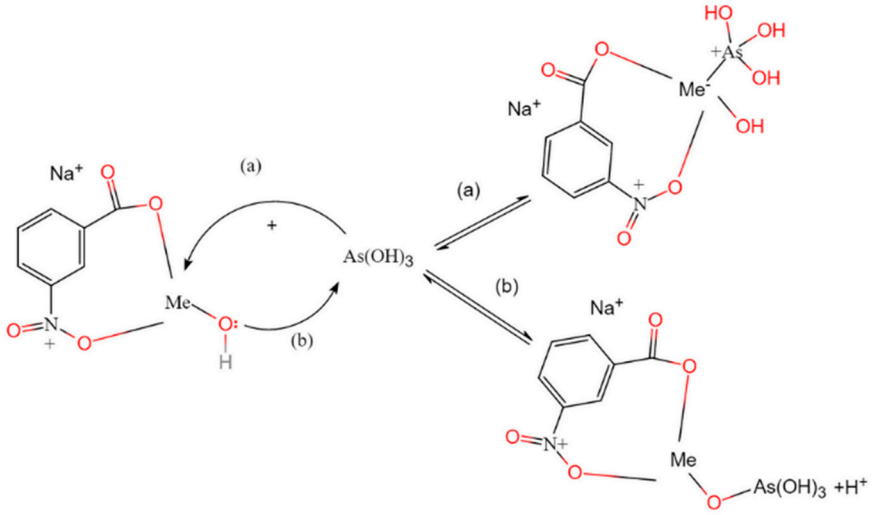

Figure 6. Possible adsorption mechanism of m-NBO on an arsenopyrite surface with two binding mechanisms involving m-NBO: a metal cation and arsenic (Me can be Fe^{3+}). a—is expected to be rather weak due to steric hindrance and repulsion of the $0H^-$ ligands and due to a small difference in Pauling's electronegativity; b—In the case of the Me-O-As bridge, a stable bond is expected.

Schaufuss et al. [34] proposed that, under high vacuum conditions, the surface reaction of oxygen and arsenopyrite is manifested as the rapid oxidation of surface arsenic particles. In the adsorption process, As and Fe react with arsenopyrite and the –COO–, –NOO– in m-NBO may cause adsorption in the complexation. Qin et al. [35] and other researchers reported that xanthate is oxidized to produce dixanthate, which increases the hydrophobicity of the mineral surface and promotes the mineral flotation. In the arsenopyrite treated with m-NBO, under the action of NaBX, no new characteristic peaks appeared on the surface of arsenopyrite and the double xanthate absorption peak at 1382 cm^{-1} disappeared. However, a weak absorption peak is present, which may be due to the symmetric stretching vibration of –NOO– at 1405 cm^{-1} and 1388 cm^{-1} of m-NBO, indicating that m-NBO and dixanthate have competitive adsorptions on the surface of arsenopyrite. Due to the flotation effect of m-NBO, the hydrophilicity of arsenopyrite increased and arsenopyrite was inhibited. This result is also consistent with the flotation test results of the arsenopyrite micro-flotation mineral.

3.3. XPS Analysis

XPS was used to study the effects of m-NBO and NaBX on the surface chemical composition and adsorption on arsenopyrite surfaces. The XPS spectra of Fe 2p, S 2p, and As 3d on the surface of arsenopyrite before and after the addition of m-NBO and NaBX are shown in Figure 7, respectively.

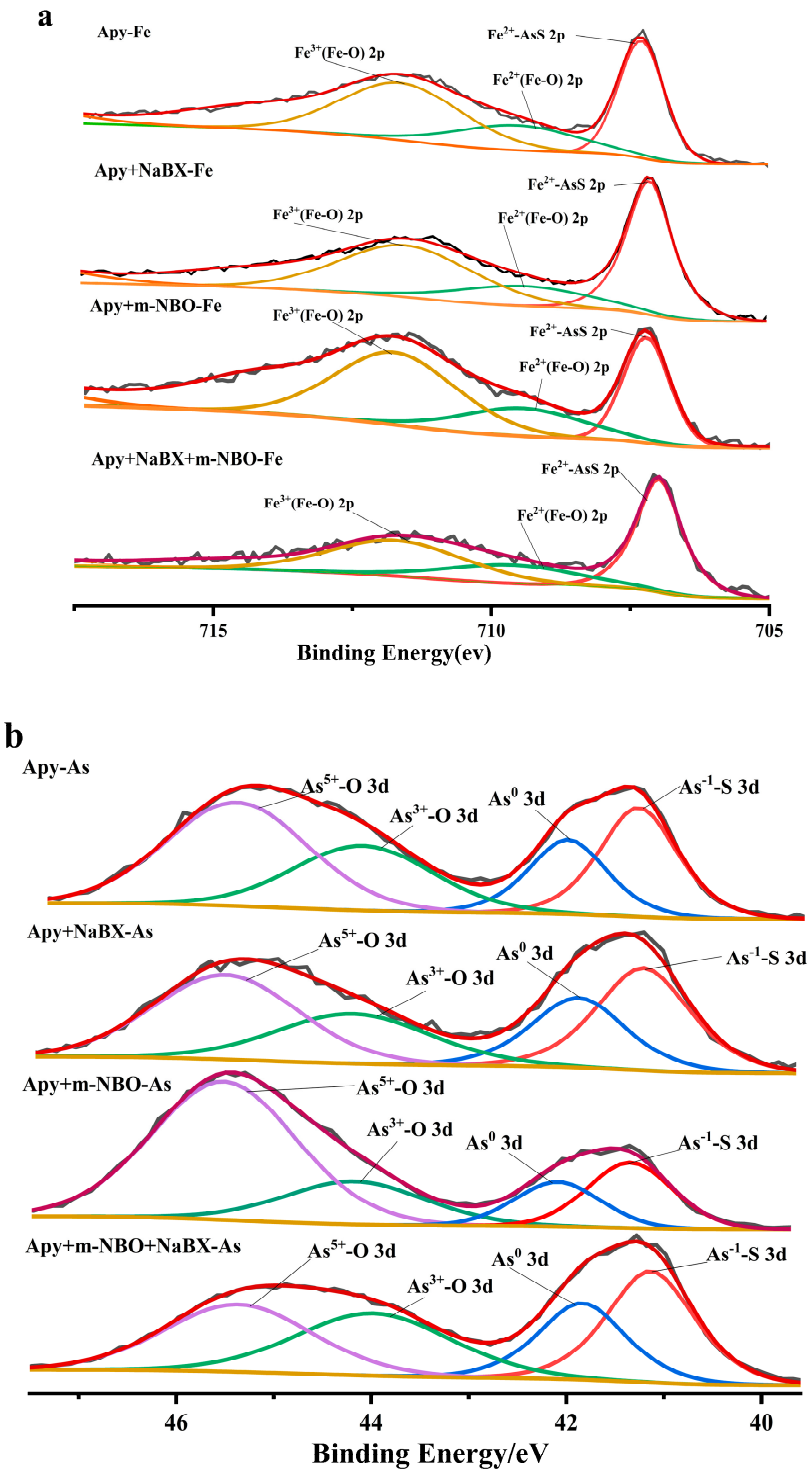

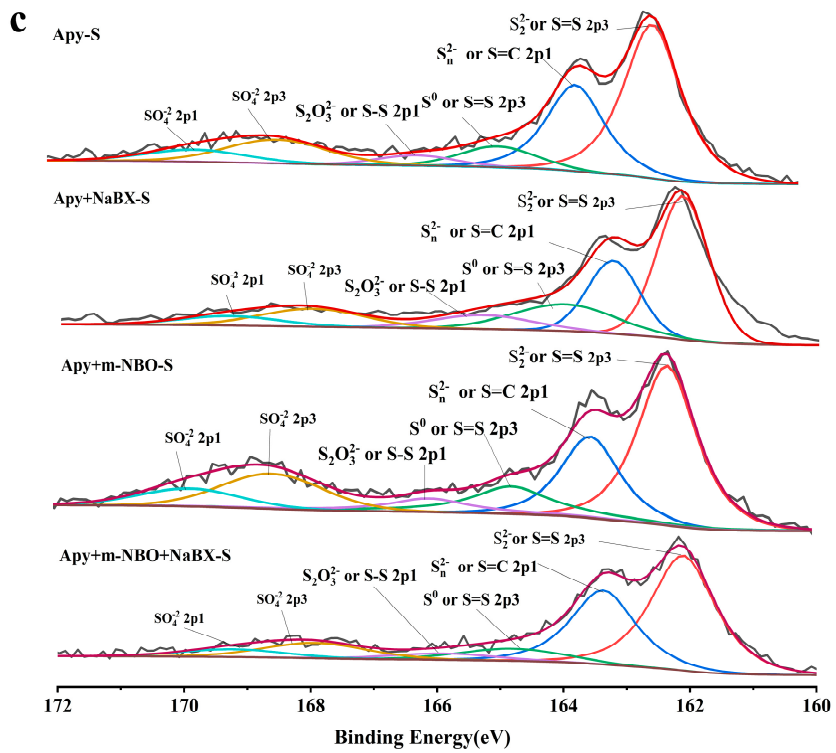

Figure 7. XPS of arsenopyrite after interactions with m-NBO and NaBX; pH = 11.5, $C_{(m\text{-}NBO)}$ = 50mg·L^{-1}, $C_{(NaBX)}$ = 1.6 × 10^{-3} mol·L^{-1}; (**a**)Fe 2p, (**b**)As 3d, (**c**)S 2p.

As shown in Figure 7a, most of the iron atoms on the surface of arsenopyrite are Fe(II) combined with As–S ion groups. As Fe(II) has almost the same binding energy when combined with As–S or S–S [36], the content of Fe(II)–AsS is used to express the total Fe(II)-As and Fe(II)–S contents. For accurate comparison of the relative species distribution changes before and after the action of arsenopyrite with m-NBO and NaBX, the same full width at half maximum was set under the same binding energy or the corresponding chemical state, as shown in Table 3.

Table 3. Distribution of the chemical state, binding energy, and atomic concentration of the surface elements Fe 2p, As 2p, and S 3d before and after the adsorption of m-NBO and NaBX on arsenopyrite. FWHW, full width at half maximum.

Chemical State	BE/eV				FWHW	Atomic/%			
	Apy	Apy+ NaBX	Apy+ m-NBO	Apy + m – NBO + NaBX		Apy	Apy+ NaBX	Apy+ m-NBO	Apy + m - NBO + NaBX
Fe^{2+}–AsS	707.3	707.1	707.3	707.0	1.0	35	43	29	41
Fe^{2+}–(Fe–O)	709.6	709.4	709.5	709.6	2.7	20	19	20	16
Fe^{3+}(Fe–O)	711.7	711.6	711.8	711.7	2.6	45	38	51	43
As^{-1}–S	41.3	41.1	41.3	41.2	1.0	39	33	26	34

As^0	42.1	41.8	42.0	41.9	1.0				
As^{3+}–O	44.2	44.0	44.1	44.2	1.7	23	26	17	33
As^{5+}–O	45.5	45.4	45.5	45.5	1.8	38	41	57	33
S_2^{2-} or S=S	162.3	162.2	162.3	162.1	1.1				
						71	74	60	62
S_n^{2-} or S=C	163.6	163.2	163.5	163.4	1.1				
S^0 or S=S	164.8	164.0	164.8	164.8	1.4				
						11	11	18	23
$S_2O_3^{2-}$ or S–S	166.1	165.3	166.1	165.9	1.4				
SO_4^{2-}	168.3	168.1	168.5	167.9	1.9				
						18	15	22	15
SO_4^{2-}	169.6	169.3	169.8	169.2	1.9				

As shown in Figure 7a, 707.3 eV [36], 709.6 eV, and 711.7 eV on the surface of arsenopyrite represent $Fe^{2+}-AsS$, $Fe^{2+}(Fe-O)$, and $Fe^{3+}(Fe-O)$, respectively, and the relative atomic concentrations are 35%, 20%, and 45%, respectively, as shown in Table 4. After the treatment of arsenopyrite and NaBX, the content of low-valence oxides of arsenopyrite increases; the content of high-valence Fe^{3+} decreases; and the relative atomic concentrations are 43%, 19%, and 38%, respectively, as shown in Table 3. The adsorption of xanthate and dixanthate on the surface of arsenopyrite forms $Fe(OH)\cdot X$ and $Fe(OH)_2\cdot X_2$, which are beneficial to the flotation of arsenopyrite [37,38]. When arsenopyrite reacts with m-NBO, the content of arsenopyrite in the Fe2p energy spectrum as $Fe^{2+}-AsS$, $Fe^{3+}-AsS$, and $Fe^{3+}(Fe-O)$ changes to varying degrees. In the low oxidation state, the content of $Fe^{2+}-AsS$ decreased by 6%, while the content of Fe^{3+}(Fe–O) increases by 6%. This may be due to the effect of m-NBO, in which the roles of –COOH– and –NOO– promote the conversion of Fe^{2+} to Fe^{3+}. Infrared absorption spectroscopy has proved that m-NBO has a complexation effect on the surface of arsenopyrite, showing that, under the action of m-NBO, the oxidation of [Fe] on the surface of arsenopyrite is promoted. When arsenopyrite reacts with m-NBO and then reacts with NaBX, the $Fe^{3+}-AsS$ concentration on the arsenopyrite surface changes a little, and the As–metal–organic complex fraction is easily formed on the arsenopyrite surface to cover the surface of arsenopyrite, preventing the adsorption of NaBX on the surface of arsenopyrite [39], showing that, under the action of m-NBO, the oxidation degree of iron ions on the surface of arsenopyrite increases, which intensifies the increase in the oxide content on the surface of arsenopyrite; due to the existence of an As–metal–organic complex fraction, the adsorption of NaBX on the surface of arsenopyrite is weakened and the recovery of arsenopyrite is reduced, which is also consistent with the results of the flotation test.

Table 4. The Tafel parameters of the electrode in the pH = 9 solution were studied (0.3 mol/L m-NBO).

Electrode	Corrosion Potential E_{corr} (mV)	Corrosion Current I_{corr} (μA/cm²)
Apy	−95.5	8.49
Apy + NaBX	−100.5	10.47
Apy + m-NBO	−101.9	8.99
Apy + m-NBO + NaBX	−165.0	7.31

Figure 7b and Table 3 show the As 3d energy spectrum and binding energy before and after the action of arsenopyrite with m-NBO and NaBX. The best fit of the As 3d spectrum of arsenopyrite produces As^{-1}–S peaks and As^{0} peaks with binding energies of 41.3 eV and 42.1 eV [4], with a relative atomic concentration of 38.55%. The As 3d energy spectrum shows that As has a high oxidation state, the peaks at 44.2eV and 45.5eV represent As^{3+}–O and As^{5+}–O [40,41], and the relative atomic concentration contents are 23% and 38%, respectively. When arsenopyrite reacts with NaBX, under alkaline conditions, the surface As^{0} and As^{5+}–O of arsenopyrite at the same binding energy do not change significantly. The content of As^{3+}–O changes greatly relative to the atom content. The As^{3+}–O concentration increases from 23% to 26%. When arsenopyrite reacts with m-NBO, the best fit of the As 3d spectrum after the addition of arsenopyrite produces As^{1-}–S peaks and As^{0} peaks with binding energies of 41.3eV and 42.0eV. The relative atomic concentration is 26%, a high oxidation state peak of As with a high binding energy appeared at 45.5eV, and the relative atomic concentration content increased from 19% to 57%. These results show that, under the action of m-NBO, the surface oxidation of arsenopyrite is intensified and the content of high oxidation state As^{5+}–O on the surface of arsenopyrite is increased. After the action of m-NBO and the subsequent action of NaBX, the surface content of arsenopyrite increases by 34%, 33%, and 33%. The discovery of the oxidation states of As^{0}, As^{3+}, and As^{5+} illustrates the continuous reaction model of arsenic oxidation: the basic electron transfer stage. This indicates that m-NBO accelerates the oxidation of arsenopyrite surfaces under alkaline conditions and increases the content of high oxidation state As^{5+}–O on arsenopyrite surfaces, which may be due to the production of AsO_3^{3-} and AsO_4^{2-} on arsenopyrite surfaces, which increases the hydrophilicity of the arsenopyrite surface, so arsenopyrite is inhibited.

Figure 7c and Table 3 show the S 2p energy spectrum and binding energy before and after the action of arsenopyrite with m-NBO and NaBX. The S 2p energy spectrum is fitted by three pairs of spin orbits. The main peaks of arsenopyrite are $(AsS)^{2-}$ with binding energies of 162.3 eV and 163.6 eV [36]. The relative atomic concentration accounts for approximately 71%. The other two peaks are at 164.8 eV and 166.1 eV binding energies. The peak is the slight oxidation product of arsenopyrite, such as elemental sulfur and polysulfide [42], with an atomic relative concentration of 11%. During the oxidation of sulfur, many intermediate oxidation products are produced. The final product is a sulfate ion. The SO_4^{2-} peaks in the oxidation state have 168.3 eV [43] and 169.6 eV binding energies, and the relative atomic concentration is 17.75%. When arsenopyrite interacts with NaBX, the binding energies of 163.6 eV shifted (−0.4 eV), indicating that NaBX is on the surface of arsenopyrite. This indicates that xanthate iron is formed on the surface of arsenopyrite. The concentration of the relative atomic concentration accounts for the arsenopyrite S 2p spectrum at $(AsS)^{2-}$ being reduced from 71% to 62%, which may be caused by the overlap in the signal from the terminal S* of dixanthogen and the disulfide signal on the surface of arsenopyrite [44]. In addition, the peak at 166.1 eV for the binding

energy in the presence of NaBX is significantly shifted (−0.8 eV), which is mainly due to dixanthate ($C_4H_9CH_2$–O=C=S*) = S–S=(*S=C–O–$CH_2C_4H_9$) in the formation of the bridge S [45]. When arsenopyrite interacts with m-NBO, the relative atomic concentration of SO_4^{2-} on the surface of arsenopyrite increases from 18% to 22%, indicating that m-NBO has a certain oxidation effect on arsenopyrite, but a certain difference is found when compared with As^{5+}–O (38~57%), indicating that SO_4^{2-} affects the hydrophobicity of arsenopyrite to a certain extent, although it is not the main reason. When arsenopyrite interacts with m-NBO, after the action of NaBX, the binding energy changes insignificantly. The binding energy does not change much at 163.6eV and 166.1eV, indicating that no formation of iron xanthogenate or dixanthate is found on the surface of arsenopyrite at this time. This difference in adsorption provides a basis for m-NBO to inhibit arsenopyrite.

The results show that the level of S_2^{2-} and its SO_4^{2-}content are factors that determine whether arsenopyrite is floatable, but m-NBO has a certain limiting effect on the degree of oxidation of S_2^{2-} under alkaline conditions. The degree of oxidation of [Fe] and [As] ions determines the hydrophilicity of the surface of arsenopyrite—the coverage of hydrophilic passivation films such as ferric hydroxide and arsenate—thereby inhibiting arsenopyrite [46].

3.4. Electrochemical Analysis

CV curves are a commonly used electrochemical research method. This method controls the scanning of the electrode potential one or more times in a triangular waveform at different rates over time. The potential range allows for different reduction and oxidation reactions to occur alternately on the electrode and for recording a current–potential curve. According to the shape of the curve, the degree of reversibility of the electrode reaction; the possibility of intermediates, phase boundary adsorption, or new phase formation; and the nature of the coupling chemical reaction can be judged. A Tafel curve is used to analyze the influence of corrosion potential mineral flotation separation during the flotation process. However, oxidation is the key step in the inhibition of arsenopyrite. As the surface oxidation reaction of sulfide minerals is essentially an electrochemical reaction, analyzing the effect of arsenopyrite on the surface of minerals through the electrochemical behavior of arsenopyrite in the slurry is of great significance [47].

As shown in Figures 8–11, the pH of arsenopyrite is at pH = 9 and pH = 11.5, and the CV curve and the Tafel curve in the solution are used to analyze the influence of m-NBO and NaBX on the flotation of arsenopyrite.

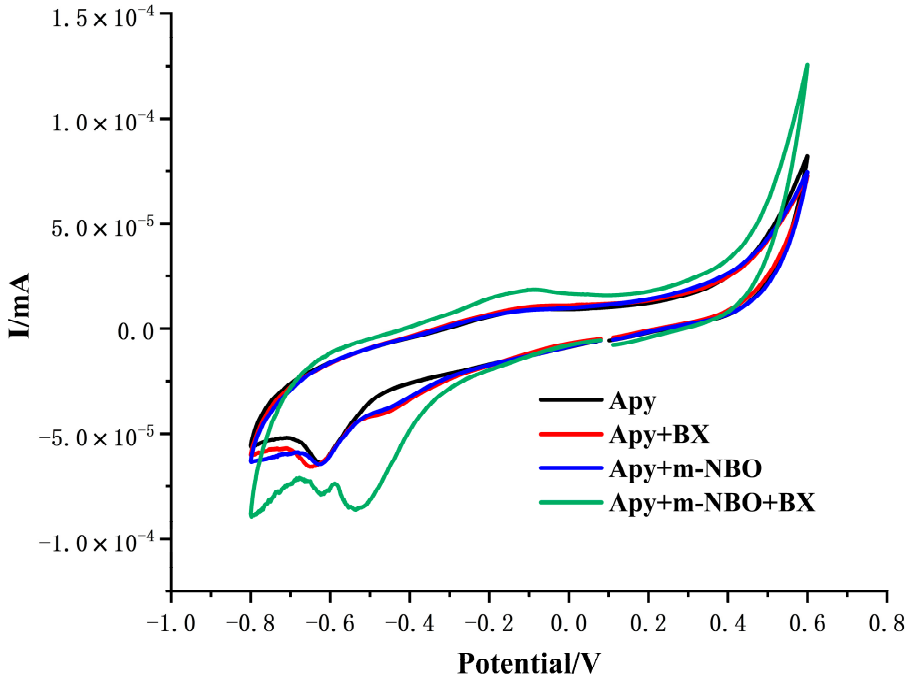

Figure 8. CV curves of the arsenopyrite electrode in the presence of m-NBO and NaBX at pH = 9; scanning rate: 10 mV/s, $C_{(m\text{-}NBO)}$ = 0.3 mol·L^{-1}, $C_{(NaBX)}$ = 1.6 × 10^{-3} mol·L^{-1}.

As shown in Figure 8, when pH = 9, the difference between arsenopyrite under natural conditions and NaBX conditions is small, but after the action of m-NBO, under the action of NaBX, the degree of oxidation on the surface of arsenopyrite increases. Compared with no NaBX, the arsenopyrite electrode has a more obvious anode peak at about −100 mV. We speculate that the peak may be due to NaBX oxidation to dixanthate, and the increase in the pH of the slurry increases the current density and accelerates the reaction, as shown in Figure 9.

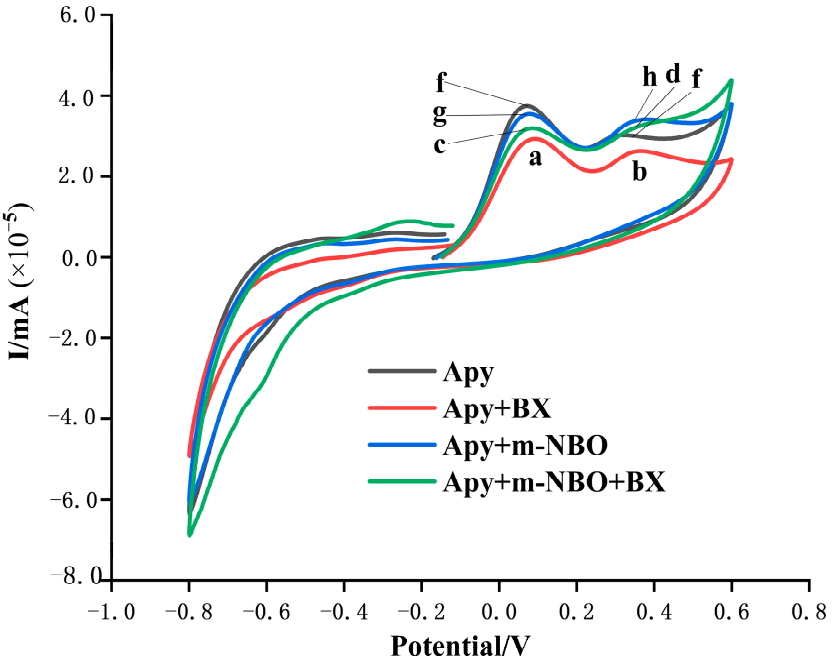

Figure 9. CV curves of the arsenopyrite electrode in the presence of m-NBO and NaBX at pH = 11.5; scanning rate: 10 mV/s, C(m-NBO) = 0.3 mol·L^{-1}, C(NaBX) = 1.6 × 10^{-3} mol·L^{-1}.

Under high alkali conditions, such as when the pH is 11, the current density of the anode peak increases significantly and the oxidation speed increases, indicating that the oxidation reaction easily proceeds, as shown in Figure 9. When m-NBO and NaBX are not present in the system, an oxidation reaction occurs on the surface of arsenopyrite in the alkaline medium, as shown in Figure 9. Since As and S are covalently bonded and are difficult to separate, the initial oxidation reaction can be expressed by Equation (3) [48]:

$$FeAsS + 3H_2O \rightarrow Fe(OH)_3 + AsS + 3H^+ + 3e^- \quad (3)$$

The production of realgar-like products (AsS) requires a higher potential for further oxidation. As shown in Figure 9, the oxidation of arsenopyrite at high potential can be expressed by Equation (4):

$$FeAsS + 7H_2O \rightarrow Fe(OH)_3 + S^0 + HAsO_4^{2-} + 10H^+ + 8e^- \quad (4)$$

The generated S^0 is an intermediate product of oxidation products SO_4^{2-}, $S_2O_3^{2-}$, SO_3^{2-}, and $S_2O_6^{2-}$. Under alkaline conditions, iron oxides and arsenates co-deposit on the surface of arsenopyrite to form a passivation film, which reduces the floatability of arsenopyrite.

As shown in Figure 9, when NaBX is added to the system, the electrochemical activity of arsenopyrite is reduced owing to the presence of dixanthate, and the process of transforming arsenopyrite surface ions to a high oxidation state is weakened. The main reason for this is that NaBX is oxidized to dixanthate. The adsorption on the surface of arsenopyrite increases the floatability of arsenopyrite. Yang et al. [49], Qin et al. [50], and others have also conducted similar studies, and they report that dixanthate is a hydrophobic entity in the flotation of sulfide minerals. The oxidation of NaBX to dixanthate is accompanied by a chemical adsorption process of electron transfer. The oxidation of acid ions on the surface of sulfide minerals to form dixanthate is carried out in two steps, as shown in Equations (5) and (6):

$$EX^- \rightleftharpoons EX_{ads} + e \quad (5)$$

$$EX_{ads}EX^- + \rightleftharpoons EX_{2ads} + e \quad (6)$$

In this process, low-valence $Fe(OH)$ and $Fe(OH)_2$ easily produce $Fe(OH) \cdot X$ and $Fe(OH) \cdot X_2$, etc. The XPS analysis showed that xanthogenate was present on the surface of arsenopyrite. The high oxidation state on the surface of arsenopyrite is reduced, and because of the electrochemical adsorption of NaBX on the surface of arsenopyrite, the electrochemically adsorbed xanthogenic acid ion and other xanthogenic acid ions combine to generate dixanthate, thereby increasing the floatability of arsenopyrite.

After arsenopyrite reacted with m-NBO, as shown in Figure 9, the curve shows a reduction peak at 0.05 V, and an obvious reduction peak at the high electrode potential of 0.38 V, indicating that arsenopyrite has been electrochemically reduced under the action of m-NBO, but the anode peak is not seen in the reverse scan, which shows that the electrochemical reaction is an irreversible reaction.

After arsenopyrite reacted with m-NBO, NaBX was added. As shown in Figure 9, under the action of m-NBO, the oxidation of arsenopyrite in the solution is increased, which promotes an increase in the oxidation potential of arsenopyrite and accelerates the oxidation rate of the surface of arsenopyrite. At this time, the oxidation potential of arsenopyrite is lower than that under natural conditions, and the following reactions occur on the surface of arsenopyrite according to Equation (7):

$$FeAsS + 3H_2O \rightarrow Fe^{3+} + S^0 + AsO_3^{3-} + 6H^+ + 6e^- \quad (7)$$

As shown in Figure 9, as the oxidation potential increases, a second oxidation peak appears near 0.45 V, which is mainly because m-NBO increases the electrochemical activity on the surface of arsenopyrite, which intensifies the oxidation of S^0 and AsO_3^{3-} into

arsenopyrite oxidation. The process of generating AsO_4^{3-} and SO_4^{2-} is shown in Equation (8):

$$FeAsS + 10H_2O \rightarrow Fe^{3+} + H_2AsO_4^- + SO_4^{2-} + 18H^+ + 12e^- \quad (8)$$

Fe^{3+} and $H_2AsO_4^-$ form a hydrophilic passivation film on the surface of arsenopyrite, as shown in Equation (9):

$$H_2AsO_4^- + H_2O + Fe^{3+} \rightarrow Fe(AsO_4) \cdot 2H_2O + 2e^- \quad (9)$$

The flotation of NaBX on the surface of arsenopyrite is weakened, and the formation of $Fe(OH) \cdot X$ and $Fe(OH) \cdot X_2$ on the surface of arsenopyrite is reduced. Therefore, arsenopyrite is suppressed.

In summary, in the presence of m-NBO, as a result of the electrochemical reaction, a hydrophilic passivation film $Fe(AsO_4) \cdot 2H_2O$ is formed on the surface of arsenopyrite. This prevents the adsorption of dixanthate and xanthogenic acid on the surface of arsenopyrite. Therefore, arsenopyrite is suppressed. When folded back and scanned at −0.1—0.8 V, the reduction peak of arsenopyrite decreases, indicating that, under the action of m-NBO and NaBX, the oxidation products on the surface of arsenopyrite are not reduced, which implies that the reaction is irreversible [51].

The reason for the sulfide mineral corrosion is the presence of a substance in the slurry solution, the reduction equilibrium potential of which is higher than the oxidation equilibrium potential of the sulfide minerals. This substance is called a depolarizer, or an oxidant, in corrosion science. The effect of m-NBO on sulfide minerals is essentially electrochemical corrosion, which is closely related to the potential of the solution in the system.

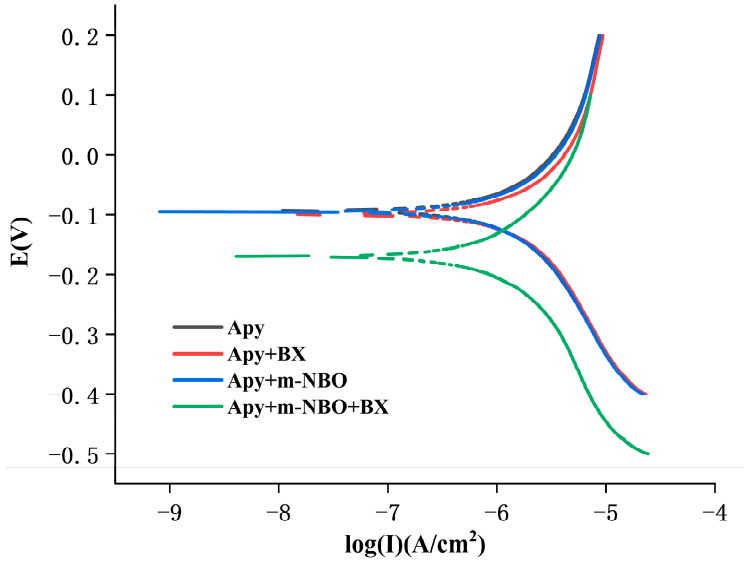

Figure 10. Tafel curves of the arsenopyrite electrode in the presence of m-NBO and NaBX at pH = 9; scanning rate: 10 mV/s, $C_{(m\text{-}NBO)}$ = 0.3 mol·L^{-1}, $C_{(NaBX)}$ = 1.6 × 10^{-3} mol·L^{-1}.

Table 4 shows the corrosion potential and the corrosion current obtained by the tangents to the two parabolas at the end of the Tafel curve at pH = 9 for [Apy], [Apy + NaBX], [Apy + m-NBO], and [Apy + m-NBO + BX], as shown in Figure 10. The coordinates of the intersection point of the two tangents are E_{corr} and I_{corr}. From the chart we can see that, from the corrosion potential, [Apy] < [Apy + NaBX] < [Apy + m-NBO] < [Apy + m-NBO + BX], and the corrosion current does not change significantly, showing that, under alkaline conditions, m-NBO has a certain inhibitory effect on arsenopyrite.

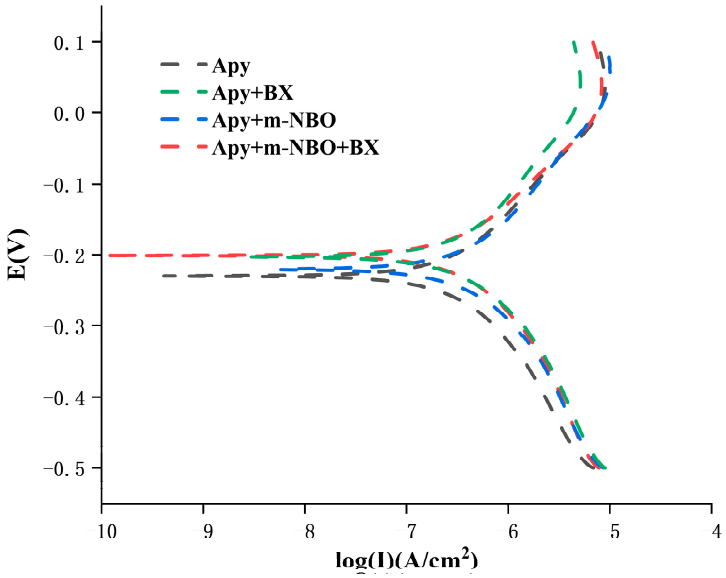

Figure 11. Tafel curves of the arsenopyrite electrode in the presence of m-NBO and NaBX at pH = 11.5; scanning rate:10 mV/s, $C_{(m\text{-}NBO)}$ = 0.3 mol·L^{-1}, $C_{(NaBX)}$ = 1.6 × 10^{-3} mol·L^{-1}.

Table 5 shows the corrosion potential and the corrosion current obtained by tangents to the two parabolas at the end of the Tafel curve under the conditions of [Apy], [Apy + NaBX], [Apy + m-NBO], and [Apy + m-NBO + NaBX], as shown in Figure 11. The coordinates of the point of intersection between the two tangents are E_{corr} and I_{corr}. From the chart, we can see that, from the corrosion potential, [Apy] < [Apy + m-NBO] < [Apy +m-NBO+ NaBX] < [Apy + NaBX]. From the corrosion current point of view, the four do not change significantly. When the other conditions are the same, the more negative the corrosion potential is, the higher the mineral surface activity, the faster the electrochemistry, and the faster the formation rate of oxidation products on the surface of arsenopyrite. Therefore, [arsenopyrite] has the worst corrosion resistance. When NaBX is added to the medium, the surface potential of arsenopyrite is obviously positively shifted. When arsenopyrite is in the action of the m-NBO added, the surface potential of arsenopyrite shifts positively, but the rate of this positive shift is significantly lower than that of [Apy + NaBX] and is 9 mV different from the E_{corr} of [Apy]. When arsenopyrite is in the action of m-NBO and NaBX is added, the surface potential of arsenopyrite shifts positively but the rate of this positive shift is lower than that of [Apy + NaBX] and is 23 mV different from the E_{corr} of [Apy] and is 4 mV different from the E_{corr} of [Apy + NaBX].

Table 5. The Tafel parameters of the electrode in the pH = 11.5 solution were studied (0.3 mol/L m-NBO).

Electrode	Corrosion Potential E_{corr} (mV)	Corrosion Current I_{corr} (μA/cm²)
Apy	−228	2.22
Apy + NaBX	−201	2.64
Apy + m-NBO	−219	2.92
Apy + m-NBO + NaBX	−205	2.49

The complexation of m-NBO forms a hydrophilic passivation film on the surface of arsenopyrite, reducing the adsorption of dixanthate on the surface of arsenopyrite, which in turn inhibits arsenopyrite. This is consistent with the flotation test results.

4. Conclusions

In this study, we discovered and thoroughly studied a new type of inhibitor: sodium nitrobenzoate (m-NBO). Its molecular structure contains multiple functional groups such as -COO– and –NOO–. The reasonable combination of multiple functional groups and a matching chain structure inhibits arsenopyrite flotation.

When NaBX is used as a collector under alkaline conditions, despite the presence of low-valence oxidation products such as H_3AsO_3, hydrophobic S_2^{2-} dominates and makes the surface of arsenopyrite floatable. After the action of m-NBO, it weakened the effects of butyl xanthate with arsenopyrite. Under alkaline conditions, high-oxidation state substances such as Fe^{3+} and AsO_4^{2-} on the surface of arsenopyrite occupy the dominant position. Consequently, the floatability of arsenopyrite is reduced.

In this study, the modification of an organic inhibitor, m-NBO, increases the oxidation potential of an arsenopyrite aqueous solution system was shown, resulting in the formation of insoluble $Fe(AsO_4) \cdot 2H_2O$ and other hydrophilic passivation films on the surface of arsenopyrite and thus preventing the adsorption of NaBX. The passivation film that formed on the surface of arsenopyrite is an irreversible reaction, and the concentration significantly exceeds the content of polysulfide on the surface of arsenopyrite, thus reducing the floatability of arsenopyrite.

However, some subjects related to agents being optimized for the structure or combination of other agents need to be studied further for this technique to be successfully applied to sulfide-rich mineral processes.

Author Contributions: X.S.: methodology, investigation, writing—original draft, and visualization. B.W.: conceptualization, resources, writing—review & editing, supervision, project administration, and funding acquisition. M.H.: conceptualization, methodology, investigation, writing—review & editing, supervision, and funding. H.Q.: conceptualization, methodology, investigation, writing—review & editing, and supervision. J.D.: discussion. J.C.: conceptualization, methodology, investigation, writing—review & editing, and supervision. X.J.: conceptualization, methodology, investigation, writing—review & editing, and supervision. All authors have read and agreed to the published version of the manuscript.

Funding: This research was funded by China Tin Group Co., Ltd.

Data Availability Statement: Not Applicable.

Acknowledgements: The authors thank Shiyanjia Lab (www.shiyanjia.com) for supporting the electrochemical measurements, and thank Yongqiang Lu for his contributions to this article.

Conflicts of Interest: The authors declare that they have no known competing financial interests or personal relationships that could have appeared to influence the work reported in this paper.

Reference

1. Rathi, B.S.; Kumar, P.S. A review on sources, identification and treatment strategies for the removal of toxic Arsenic from water system. J. Hazard. Mater. **2021**, *418*, 126299. https://doi.org/10.1016/j.jhazmat.2021.126299.
2. Mandaliev, P.N.; Mikutta, C.; Barmettler, K.; Kotsev, T.; Kretzschmar, R. Arsenic Species Formed from Arsenopyrite Weathering along a Contamination Gradient in Circumneutral River Floodplain Soils. Environ. Sci. Technol. **2013**, *48*, 208–217. https://doi.org/10.1021/es403210y.
3. Corkhill, C.; Vaughan, D. Arsenopyrite oxidation—A review. Appl. Geochem. **2009**, *24*, 2342–2361. https://doi.org/10.1016/j.apgeochem.2009.09.008.
4. Buckley, A.N.; Walker, G.W. The surface composition of arsenopyrite exposed to oxidizing environments. Appl. Surf. Sci. **1988**, *35*, 227–240. https://doi.org/10.1016/0169-4332(88)90052-9.
5. Park, I.; Higuchi, K.; Tabelin, C.B.; Jeon, S.; Ito, M.; Hiroyoshi, N. Suppression of arsenopyrite oxidation by microencapsulation using ferric-catecholate complexes and phosphate. Chemosphere **2021**, *269*, 129413. https://doi.org/10.1016/j.chemosphere.2020.129413.

6. Chen, H.; Li, B.; Zhang, B. Decomposition of pyrite and the interaction of pyrite with coal organic matrix in pyrolysis and hydropyrolysis. Fuel **2000**, *79*, 1627–1631. https://doi.org/10.1016/S0016-2361(00)00015-6
7. Alonso, D.L.; Latorre, S.; Castillo, E.; Brandão, P.F. Environmental occurrence of arsenic in Colombia: A review. Environ. Pollut. **2014**, *186*, 272–281. https://doi.org/10.1016/j.envpol.2013.12.009.
8. Ma, X.; Bruckard, W. Rejection of arsenic minerals in sulfide flotation—A literature review. Int. J. Miner. Process. **2009**, *93*, 89–94. https://doi.org/10.1016/j.minpro.2009.07.003.
9. Bruckard, W.; Davey, K.; Jorgensen, F.; Wright, S.; Brew, D.; Haque, N.; Vance, E. Development and evaluation of an early removal process for the beneficiation of arsenic-bearing copper ores. Miner. Eng. **2010**, *23*, 1167–1173. https://doi.org/10.1016/j.mineng.2010.03.015.
10. Harmer, S.; Nesbitt, H. Stabilization of pyrite (FeS_2), marcasite (FeS_2), arsenopyrite (FeAsS) and loellingite ($FeAs_2$) surfaces by polymerization and auto-redox reactions. Surf. Sci. **2004**, *564*, 38–52. https://doi.org/10.1016/j.susc.2004.06.199.
11. Aylmore, M.G.; Lincoln, F.J. Mechanical milling of auriferous arsenopyrite and pyrite. J. Alloy. Compd. **1996**, *242*, 22–34. https://doi.org/10.1016/0925-8388(96)02383-3.
12. Qiu, T.; Zhang, B.; Zhang, W. Current status and progress of technology of separating arsenopyrite and pyrite. Min. Process. Equip. **2013**, *41*, 1–5.
13. Xiong, D.L.; Yue-Hua, H.U.; Zhi-Guo, H.E. Advances in Research on Organic Depressor's Depressing of Arsenopyrite in Sulfide Flotation. Min. Metall. Eng. **2004**, *24*, 42–44.
14. Chen, Y.; Yang, H.; Liu, Y.; Chen, G. Structural evolution of arsenopyrite and dearsenification by mechanical activation. J. Environ. Chem. Eng. **2021**, *9*, 104682. https://doi.org/10.1016/j.jece.2020.104682.
15. Guo, B.; Lin, X.; Fu, W.; Ku, J. Establishment of electrochemical methods to examine the adsorption of flotation surfactants onto a mineral surface. J. Chem. Technol. Biotechnol. **2020**, *95*, 1580–1589. https://doi.org/10.1002/jctb.6353.
16. Li, G.; Zhang, H.; Shinnosuke, U. Surface chemical compositions of arsenopyrite and pyrite particles. Nonferrous Met. **1992**, *44*, 25–29.
17. Beattie, M.; Poling, G. A study of the surface oxidation of arsenopyrite using cyclic voltammetry. Int. J. Miner. Process. **1987**, *20*, 87–108. https://doi.org/10.1016/0301-7516(87)90019-6.
18. Qiang, L.; Jin, H. Preparation of some new micromolecular organic depressants and their reactivty to pyrite and arsenopyrite. J. Cent. South Univ. **1991**, *22*, 256–262.
19. Chen, J.; Feng, Q.; Yiping, L.U. Structure of organic depressants and its depressing on sulfide minerals. Nonferrous Met. **1998**, *50*, 61–65.
20. Liu, Z.S.; Fu-Chu, W.U.; Lun, S.X. The Research Status and Development for Flotation Separation of Pyrite and Arsenopyrite. Yunnan Metall. **2015**, *44*, 12–17.
21. Zhao, Z.Q.; Ren, L.D. Separation of Arsenopyrite from Pyrite by Reverse Flotation. Multipurp. Util. Miner. Resour. **2000**, 7–12. doi:10.3969/j.issn.1000-6532.2000.02.003.
22. Liu, R.; Li, J.; Wang, Y.; Liu, D. Flotation separation of pyrite from arsenopyrite using sodium carbonate and sodium humate as depressants. Colloids Surf. A: Physicochem. Eng. Asp. **2020**, *595*, 124669. https://doi.org/10.1016/j.colsurfa.2020.124669.
23. Andrá, P.; Kunierová, M.; Adam, M.; Slesarova, A.; Chovan, M. Biological-chemical oxidation of ore minerals at the Pezinok deposit (Male Karpaty Mts., Western Carpathians Slovakia). *Inz. Miner.* **2009**, *10*, 1–26.
24. Min, Z.H.; Bing, Q.Y.; Dan, F. A study on inhibitive action of sodium p-nitrobenzoate for corrosion of carbon steel. Oilfield Chem. **1996**, *13*, 70–73.
25. Boctor, N.Z. Mineral Chemistry of Metal Sulfides; Earth-Science Reviews. **1980**, *15*, 410–411. https://doi.org/10.1016/0012-8252(80)90122-1.
26. Liu, X.; Li, Q.; Zhang, Y.; Jiang, T.; Yang, Y.; Xu, B.; He, Y. Electrochemical behaviour of the dissolution and passivation of arsenopyrite in 9K culture medium. Appl. Surf. Sci. **2020**, *508*, 145269. https://doi.org/10.1016/j.apsusc.2020.145269.
27. Redkina, G.V.; Sergienko, A.S.; Kuznetsov, Y.I. Effect of sodium dodecylphosphonate and its composition with sodium m-nitrobenzoate on anodic behavior of zinc in chloride-containing borate buffer. Corros. Mater. Prot. **2019**, 2019. https://doi.org/10.31044/1813-7016-2019-0-9-25-32.
28. Yuwang, X. Mineralogical Study of a Polymetallic Sulfide Ore in Inner Mongolia. Nonferrous Met. Miner. Process. Sect. **2019**, *1*, 6–13. https://doi.org/10.3969/j.issn.1671-9492.2019.01.002.
29. Ning, S.; Li, G.; Shen, P.; Zhang, X.; Li, J.; Liu, R.; Liu, D. Selective separation of chalcopyrite and talc using pullulan as a new depressant. Colloids Surf. A: Physicochem. Eng. Asp. **2021**, *623*, 126764. https://doi.org/10.1016/j.colsurfa.2021.126764.
30. Cao, Z.; Wang, P.; Zhang, W.; Zeng, X.; Cao, Y. Mechanism of sodium sulfide on flotation of cyanide-depressed pyrite. Trans. Nonferrous Met. Soc. China **2020**, *30*, 484–491. https://doi.org/10.1016/s1003-6326(20)65228-1.
31. Wang, X.-H. Interfacial Electrochemistry of Pyrite Oxidation and Flotation. 1: Effect of borate on pyrite surface oxidation. J. Colloid Interface Sci. **1996**, *178*, 628–637. https://doi.org/10.1006/jcis.1996.0160.
32. Janczak, J. Structure and phase transition in 1-(diaminomethylene)thiouron-1-ium m-nitrobenzoate monohydrate and the structure of its anhydrous deuterated analogue. J. Mol. Struct. **2021**, *1230*, 129626. https://doi.org/10.1016/j.molstruc.2020.129626.
33. Fuerstenau, M.C.; Kuhn, M.C.; Elgillani, D.A. The role of dixanthogen in xanthate flotation of pyrite. Trans. AIME **1968**, *241*, 148–156.
34. Schaufuss, A.G.; Nesbitt, H.W.; Scaini, M.J.; Hoechst, H.; Bancroft, M.G.; Szargan, R. Reactivity of surface sites on fractured arsenopyrite (FeAsS) toward oxygen. American Mineralogist **2000**, *85*, 1754–1766.

35. Qin, W.-Q.; Wang, X.-J.; Ma, L.-Y.; Jiao, F.; Liu, R.-Z.; Gao, K. Effects of galvanic interaction between galena and pyrite on their flotation in the presence of butyl xanthate. Trans. Nonferrous Met. Soc. China **2015**, *25*, 3111–3118. https://doi.org/10.1016/s1003-6326(15)63940-1.
36. Nesbitt, H.; Muir, I.; Prarr, A. Oxidation of arsenopyrite by air and air-saturated, distilled water, and implications for mechanism of oxidation. Geochim. Cosmochim. Acta **1995**, *59*, 1773–1786. https://doi.org/10.1016/0016-7037(95)00081-a.
37. Wang, X.-H.; Forssberg, K.E. Mechanisms of pyrite flotation with xanthates. Int. J. Miner. Process. **1991**, *33*, 275–290. https://doi.org/10.1016/0301-7516(91)90058-q.
38. Yang, J. Changsha, China. Oxidation kinetics of xanthate at the surface of pyrite and arsenopyrite. J. Cent. South Univ. Technol. **1995**, *26*, 600–604.
39. Lin, H.-T.; Wang, M.; Li, G.-C. Complexation of arsenate with humic substance in water extract of compost. Chemosphere **2004**, *56*, 1105–1112. https://doi.org/10.1016/j.chemosphere.2004.05.018.
40. Zhu, T.; Lu, X.; Liu, H.; Li, J.; Zhu, X.; Lu, J.; Wang, R. Quantitative X-ray photoelectron spectroscopy-based depth profiling of bioleached arsenopyrite surface by Acidithiobacillus ferrooxidans. Geochim. Cosmochim. Acta **2014**, *127*, 120–139. https://doi.org/10.1016/j.gca.2013.11.025.
41. Mizokawa, Y. Quantitative Chemical Depth Profiles of anodic Oxide on GaAs Obtained by X-Ray Photoelectron Spectroscopy. Journal of The Electrochemical Society.**1979**, *126*, 1370–1374. https://doi.org/chin.197950022.
42. Fornasiero, D.; Li, F.; Ralston, J.; Smart, R.S. Oxidation of Galena Surfaces. J. Colloid Interface Sci. **1994**, *164*, 333–344. https://doi.org/10.1006/jcis.1994.1175.
43. Costa, M.; Rego, A.B.D.; Abrantes, L. Characterization of a natural and an electro-oxidized arsenopyrite: A study on electrochemical and X-ray photoelectron spectroscopy: I. X-ray photoelectron spectroscopic and dissolution kinetics studies. Int. J. Miner. Process. **2002**, *65*, 83–108. https://doi.org/10.1016/s0301-7516(01)00059-x.
44. Deng, M.; Karpuzov, D.; Liu, Q.; Xu, Z. Cryo-XPS study of xanthate adsorption on pyrite. Surf. Interface Anal. **2013**, *45*, 805–810. https://doi.org/10.1002/sia.5165.
45. Mikhlin, Y.; Karacharov, A.; Tomashevich, Y.; Shchukarev, A. Cryogenic XPS study of fast-frozen sulfide minerals: Flotation-related adsorption of n -butyl xanthate and beyond. J. Electron Spectros. Relat. Phenom. **2016**, *206*, 65–73. https://doi.org/10.1016/j.elspec.2015.12.003.
46. Sisenov, G.K.; Bogdanovskaya, V.A.; Tarasevich, M.R. Redox reactions of arsenopyrite in aqueous electrolyte solutions. Sov. Electrochem. **1988**, *24*, 729–733.
47. Guo, H.; Yen, W.-T. Effect of cell design and electrode configuration on the efficiency of applied potential and sulfide mineral flotation. Miner. Eng. **2003**, *16*, 877–880. https://doi.org/10.1016/s0892-6875(03)00211-5.
48. Wang, X.-H.; Ahlberg, E.; Forssberg, K.S.E. Electrochemical study of surface oxidation and collectorless flotation of arsenopyrite. J. Appl. Electrochem. **1992**, *22*, 1095–1103. https://doi.org/10.1007/bf01029592.
49. Monte, M.; Dutra, A.; Albuquerque, C.; Tondo, L.; Lins, F. The influence of the oxidation state of pyrite and arsenopyrite on the flotation of an auriferous sulphide ore. Miner. Eng. **2002**, *15*, 1113–1120. https://doi.org/10.1016/s0892-6875(02)00177-2.
50. Qin, W.; Qiu, G.; Jing, X.U.; Wang, D. Electrochemical behavior of pyrite in the prensence of xanthate solution i. electrodeposit of dixanthogen at surface of pyrite electrode. Nonferrous Met. **1999**, *51*, 26–29.
51. Sun, Z.J.; Hu, J.B.; Qian, Y.G.; Lu, Y.Q.; Li, Q.L. Studies on the Electrochemical Behavior of Methotrexate and Its ApplicationatCo/GC Ion Implantation Modified Electrode. Chem. J. Chin. Univ. **2002**, *23*, 541–545. https://doi.org/10.1007/s11670-002-0022-7.